UNIVERSITY *of York*

This is a repository copy of *An Improved Delay-Suppressed Sliding-Mode Observer for Sensorless Vector-Controlled PMSM*.

Article:

White Rose
university consortium
Universities of Leeds, Sheffield & York

An Improved Delay-Suppressed Sliding Mode Observer for Sensorless Vector-Controlled PMSM

Chao Gong, *Student Member, IEEE*, Yihua Hu, *Senior Member, IEEE*, Jinqiu Gao, *Student Member, IEEE*, Yangang Wang, *Senior Member, IEEE*, Liming Yan, *Student Member, IEEE*

Abstract— **This paper presents a delay-suppressed sliding mode observer (SMO) to observe the real-time rotor position of a permanent magnet synchronous machine (PMSM) controlled by vector control (VC) algorithms. Firstly, in order to solve the low pass filter (LPF) delay problem existing in the traditional signum function-based sliding mode observer (SMO), a brand-new hyperbolic function is initially selected as the switching function. Because a hyperbolic function with proper boundary layer is capable of reducing the chattering phenomenon of a SMO, it is not necessary to re-employ LPFs to eliminate the adverse impacts of chattering on the position estimation accuracy. In order to ensure the reachability and stability of the hyperbolic function-based SMO, the observer gain is calculated by the means of a Lyapunov function in this paper. Secondly, to solve the problem of calculation delay caused by digital computation, a current pre-compensation scheme based on dual-sampling strategy in one switching period is proposed. After compensating the calculation delay, the accuracy of position estimation as well as the motor control performance can be improved. Finally, the proposed SMOs with and without delay compensation are verified by both simulation and experiments which are conducted on a three-phase 1.5kW PMSM drive prototype.**

Index Terms— **Permanent magnet synchronous machine, sensorless control, sliding mode observer, switching function, delay compensation.**

I. INTRODUCTION

D UE to the advantages of high power density, high efficiency, simple structure and wide speed range,

C. Gong and Y. Hu are with the Department of Electrical Engineering and Electronics, University of Liverpool, Liverpool L69 3GJ, U.K. (E-mail: 1452101806@qq.com, y.hu35@liverpool.ac.uk).

J. Gao is with the School of Automation, Northwestern Polytechnical University, and Shaanxi Key Laboratory of Small & Special Electrical Machine and Drive Technology, Xi'an 710129, China (e-mail: 592577899@qq.com).

Y. Wang is with the R&D Centre of CRRC Dynex Semiconductor Ltd, Lincoln LN6 3LF, U.K. (E-mail: Yangang.Wang@dynexsemi.com).

L. Yan is with the School of Automobile, Chang'an University, Xi'an 710064, China. (E-mail: liming123@mail.nwpu.edu.cn).

permanent magnet synchronous machines (PMSM) have drawn increasing attention in the computer numerical control (CNC) machine tools, elevator control and traction drives [1]-[6]. To take full advantage of these superior electromechanical tools, many high-performance control strategies have been cooperatively developed, the most popular of which is vector control (VC) [7]-[9]. In practice, since a PMSM receives sinusoidal magnetic flux from the permanent magnets (PM) mounted on/in the rotor, it is necessary to obtain the precise rotor position and speed for normal control [10]. Usually, the required information can be measured by position sensors, such as resolvers and encoders. Whereas，it is well-known that the cost would goes up while the system reliability gets reduced by the use of those extra position detection and signal processing devices [11]-[14]. At present, the most effective solution to the problem is to employ sensorless control techniques to estimate the rotor position as well as the rotating speed for VC.

Sensorless control technologies can be classified into two principal categories: back electromotive force (EMF)-based method for high-speed range and saliency-tracking-based method for low-speed range. They have been investigated for decades [15]-[19]. Now, among the commonly used high-speed targeted algorithms which include Luenberger observer, extended Kalman filter and sliding mode observer (SMO), etc., SMO is especially well-known for its robustness and thus has been broadly adopted [20], [21]. However, the conventional SMO used for VC has the problem of low-pass filter (LPF) delay and calculation delay, deteriorating the accuracy of position estimation and further the drive control performance.

a) LPF delay

The conventional SMO uses the signum function as the switching function [22]-[24], leading to inevitable chattering phenomenon when the system states go through the sliding surface (SS) from one side to the other. In order to attenuate the adverse effect of chattering on the accuracy of position calculation, the LPFs with fixed or variable cut-off frequency are commonly adopted [23], [24]. However，the inherent delay attribute of the LPFs would bring about errors between the real and estimated values. At the moment, an additional position compensator which is related to the rotating speed should be designed, as in [25]. The main defect of this method is that the sensorless control topology as well as the implementation
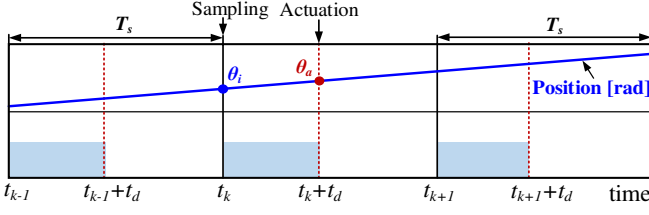
Fig. 1. Calculation delay of vector control.

becomes complex. On this ground many scholars have studied the schemes that can reduce the chattering effects without using LPFs that are endowed with delay properties. High-order SMOs have been proven to be effective on solving the LPF problems, but the observer design complexity increases dramatically because more parameters are needed to be tuned [26], [27]. [28] and [29] have proposed relatively simple solutions by just replacing the discontinuous signum function with a continuous saturation or sigmoid function depending on the boundary layer (BL) law. However, literature [30] demonstrates that the saturation-function-based method in [28] is not very satisfactory because the chattering might still exist with large uncertainties, and a fuzzy system which acts like a saturation function with a nonlinear slope inside the BL is presented to tackle the problem. But in practice, it is usually tedious to tune the parameters of a fuzzy system. Although the slope of the sigmoid function in [29] is nonlinear, paving a way for developing the novel SMOs without using LPFs, the stability analysis and observer parameter design process should be further discussed.

b) Calculation Delay

Now, digital processors are often used in PMSM drives to process the status information, execute control algorithms and generate control signals. However, a typical feature of this kind of digital system is "*one step delay*" caused by a large number of calculations [31]-[34]. In terms of the VC-based algorithms which include *abc/dq* and *dq/αβ* transformation, speed and current regulation, and complicated space vector PWM (SVPWM) computation procedures, the real actuation moment will always lag behind the measurement (sampling) point by t_d within one switching period T_s, as in Fig.1. When the traditional SMO uses the sampling currents at t_k to estimate position, θ_i can be obtained but when the SVPWM signals are applied, the rotor will rotate forward to θ_a. In this case, the machine performance, especially the load capability, might be degraded. And theoretically, the adverse effect of calculation delay will get more significant as the speed increases. Yet there are few researchers paying attention to this problem.

In order to solve the LPF and calculation delay problems, this paper proposes an improved SMO for PMSM sensorless vector control. A continuous hyperbolic function (upper and lower limits are 1 and -1, respectively) with innate nonlinear property is selected to serve as the switching function. Without using a LPF to eliminate chattering, the filter delay can be avoided. In order to analyze the stability of the new SMO, a Lyapunov function is constructed and an elaborated stability condition is innovatively obtained by contrast with the scheme in [29]. Besides, the calculation delay is compensated by using a current pre-compensation method based on dual-sampling

technique in one switching period, improving the accuracy of position estimation. On these grounds the structure of the rest of the paper is as follows. Section II describes the PMSM model and the conventional signum function-based SMO. Section III describes the proposed SMO. Particularly, the hyperbolic function and the observer's stability are analyzed in detail. In Section IV, a current pre-compensation method for removing the calculation delay is discussed. The results of the simulation and experimental verifications are presented in Section V, and Section VI presents the conclusion part.

II. CONVENTIONAL SMO

A. PMSM Modeling

The mathematical model of IPMSM in the $\alpha\beta$ stationary reference frame is expressed by the following differential equations, where the iron saturation, magnetic flux leakage, eddy current and hysteresis loss are assumed to be negligible:

$$\begin{bmatrix} \dfrac{di_\alpha}{dt} \\ \dfrac{di_\beta}{dt} \end{bmatrix} = \begin{bmatrix} -\dfrac{R_s}{L_s} & 0 \\ 0 & -\dfrac{R_s}{L_s} \end{bmatrix} \begin{bmatrix} i_\alpha \\ i_\beta \end{bmatrix} + \begin{bmatrix} \dfrac{1}{L_s} & 0 \\ 0 & \dfrac{1}{L_s} \end{bmatrix} \begin{bmatrix} u_\alpha \\ u_\beta \end{bmatrix} + \begin{bmatrix} -\dfrac{1}{L_s} & 0 \\ 0 & -\dfrac{1}{L_s} \end{bmatrix} \begin{bmatrix} e_\alpha \\ e_\beta \end{bmatrix} \quad (1)$$

where i_α, i_β, e_α, e_β and u_α, u_β represent the current, back EMF, and voltage for each phase in the stationary reference frame, respectively. R_s and L_s are the stator resistance and inductance, respectively.

The back EMF for each phase can be represented in the fixed-frame as:

$$\begin{bmatrix} e_\alpha \\ e_\beta \end{bmatrix} = \begin{bmatrix} -\dfrac{\sqrt{3}}{2}\Psi_f p\omega_m \sin\theta \\ \dfrac{\sqrt{3}}{2}\Psi_f p\omega_m \cos\theta \end{bmatrix} \quad (2)$$

Where Ψ_f is the permanent magnet flux linkage, ω_m is the rotor mechanical angular speed, p is the number of pole pairs and θ is the angular rotor position. It can be noticed that the α-, β-axis back EMF contains the real rotor position θ, but they cannot be measured directly. On this ground a sliding mode variable structure controller will be employed to extract the position information.

B. Conventional Signum-Function-based SMO

The back EMF based SMO of the PMSM system (1) can be represented as:

$$\begin{bmatrix} \dfrac{di_\alpha^*}{dt} \\ \dfrac{di_\beta^*}{dt} \end{bmatrix} = \begin{bmatrix} -\dfrac{R_s}{L_s} & 0 \\ 0 & -\dfrac{R_s}{L_s} \end{bmatrix} \begin{bmatrix} i_\alpha^* \\ i_\beta^* \end{bmatrix} + \begin{bmatrix} \dfrac{1}{L_s} & 0 \\ 0 & \dfrac{1}{L_s} \end{bmatrix} \begin{bmatrix} u_\alpha \\ u_\beta \end{bmatrix} - \begin{bmatrix} \dfrac{k}{L_s} & 0 \\ 0 & \dfrac{k}{L_s} \end{bmatrix} \begin{bmatrix} F(\bar{i}_\alpha) \\ F(\bar{i}_\beta) \end{bmatrix} \quad (3)$$

where i_α^*, i_β^* are the estimated current in the stationary reference frame. $\bar{i}_\alpha$ and $\bar{i}_\beta$ represent the errors between the estimated currents and the real currents, that is, $\bar{i}_\alpha = i_\alpha^* - i_\alpha$ and $\bar{i}_\beta = i_\beta^* - i_\beta$. For a traditional SMO, $F(\bar{i}_\alpha)$ and $F(\bar{i}_\beta)$ are signum functions, namely,
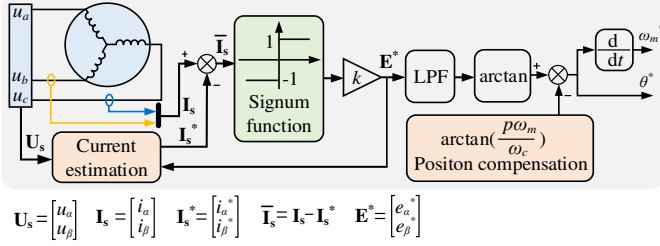
Fig. 2. Structure of the conventional SMO.

$$\begin{bmatrix} F(\overline{i_\alpha}) \\ F(\overline{i_\beta}) \end{bmatrix} = \begin{bmatrix} \text{sign}(\overline{i_\alpha}) \\ \text{sign}(\overline{i_\beta}) \end{bmatrix} \qquad (4)$$

k is the observer gain, and in order to maintain the SMO stable, it should satisfy the following inequality condition:

$$k \geq \max(|e_\alpha|, |e_\beta|) \qquad (5)$$

According to the equations (1) and (3), the estimated back EMF e_α^* and e_β^* can be written as:

$$\begin{bmatrix} e_\alpha^* \\ e_\beta^* \end{bmatrix} = k \cdot \begin{bmatrix} F(\overline{i_\alpha}) \\ F(\overline{i_\beta}) \end{bmatrix} = k \cdot \begin{bmatrix} \text{sign}(\overline{i_\alpha}) \\ \text{sign}(\overline{i_\beta}) \end{bmatrix} \qquad (6)$$

In order to attenuate the chattering effect, e_α^* and e_β^* will pass through a LPF to filter out the high-order harmonics before they are used to calculate position, as in Fig.2. Then, to compensate the delay introduced by the LPF, an extra term $\Delta\theta$ is added to the calculated value to obtain the final position and speed information (θ^*, ω_m^*):

$$\Delta\theta = \arctan(\frac{p\omega_m}{\omega_c}) \qquad (7)$$

where ω_c is the cut-off frequency of LPF and p is the number of pole pairs. In this case, the maximum angle of lag is $\dfrac{\pi}{4}$ when the electrical angular velocity $p\omega_m$ approaches ω_c.

It should be noticed that for the traditional SMO based on signum function, the LPF must be used for chattering reduction and the delay compensation part should be employed to reduce the impacts from the LPF, which complicates the structure of the SMO. Consequently, it is valuable to develop novel observers without using LPFs, and then the compensator is dismissed completely.

III. IMPROVED SMO WITHOUT USING LPF

Fundamentally, the LPF delay issue of the classic SMO arises from the chattering effect disposition method, so an effective solution is to reduce the undesirable chattering without using a LPF. This section proposes a novel SMO which utilizes a hyperbolic function as the switching function, requiring neither a LPF nor an extra compensator any longer.

A. Hyperbolic Function

With reference to literature [30], this paper aims to reduce the chattering phenomenon of SMO by smoothing out the control discontinuity and the step change within a BL near the sliding surface. To achieve this target and obtain better performance, the switching function should satisfy the following requirements:
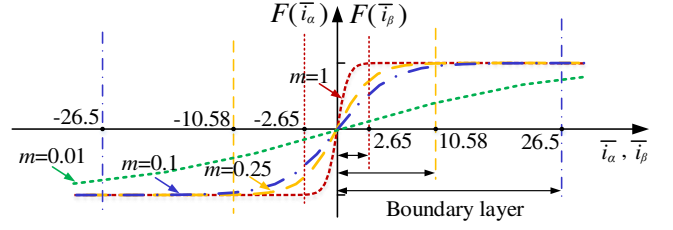
Fig. 3. Boundary layers under different values of m.

a) The function is continuous.
b) Referring to the saturation function, the upper and lower limit are 1 and -1.
c) The slope within the BL is nonlinear.
d) The function has no time-delay characteristic.

A hyperbolic function with the expression of (8) is totally qualified, so it will be used in the new SMO.

$$\begin{bmatrix} F(\overline{i_\alpha}) \\ F(\overline{i_\beta}) \end{bmatrix} = \begin{bmatrix} \dfrac{e^{m\overline{i_\alpha}} - e^{-m\overline{i_\alpha}}}{e^{m\overline{i_\alpha}} + e^{-m\overline{i_\alpha}}} \\ \dfrac{e^{m\overline{i_\beta}} - e^{-m\overline{i_\beta}}}{e^{m\overline{i_\beta}} + e^{-m\overline{i_\beta}}} \end{bmatrix} \qquad (8)$$

where m is a positive constant used for regulating the BL which is defined as the magnitude of the independent variable when $F=0.99$, as in Fig.3. Substitute (8) into (3), the improved SMO model used for e_α^* and e_β^* estimation can be eventually established.

B. Stability Analysis

Since a new switching function is adopted in the SMO, it is crucial to reappraise the stability of the observer. For the new SMO, the defined α, β-axis sliding surfaces (S_α, S_β) are $\overline{i_\alpha}$ and $\overline{i_\beta}$ which can be denoted as:

$$S = \begin{bmatrix} S_\alpha \\ S_\beta \end{bmatrix} = \begin{bmatrix} \overline{i_\alpha} \\ \overline{i_\beta} \end{bmatrix} \qquad (9)$$

To ensure the stability of the designed observer, the following equation is necessary based on Lyapunov function:

$$V = \frac{1}{2} \cdot S^T \cdot S = \frac{1}{2}\overline{i_\alpha}^2 + \frac{1}{2}\overline{i_\beta}^2 \qquad (10)$$

Obviously, $V > 0$. Then, according to the Lyapunov stability decision theorem, only by deducing $\dfrac{dV}{dt} < 0$ can we conclude that the SMO can reach a stable state. Take the time derivative of equation (10):

$$\frac{dV}{dt} = S^T \cdot \frac{dS}{dt} = \overline{i_\alpha}\frac{d\overline{i_\alpha}}{dt} + \overline{i_\beta}\frac{d\overline{i_\beta}}{dt} \qquad (11)$$

Substitute (1) and (3) into (11), it can be further derived as:

$$\frac{dV}{dt} = \begin{bmatrix} \overline{i_\alpha} & \overline{i_\beta} \end{bmatrix} \begin{bmatrix} -\dfrac{R_s}{L_s}\overline{i_\alpha} + \dfrac{1}{L_s}(e_\alpha - kF(\overline{i_\alpha})) \\ -\dfrac{R_s}{L_s}\overline{i_\beta} + \dfrac{1}{L_s}(e_\beta - kF(\overline{i_\beta})) \end{bmatrix} \qquad (12)$$

And the polynomial expression of (12) is:

$$\mathbf{U_s} = \begin{bmatrix} u_\alpha \\ u_\beta \end{bmatrix} \quad \mathbf{I_s} = \begin{bmatrix} i_\alpha \\ i_\beta \end{bmatrix} \quad \mathbf{I_s^*} = \begin{bmatrix} i_\alpha^* \\ i_\beta^* \end{bmatrix} \quad \mathbf{\tilde{I}_s = I_s - I_s^*} \quad \mathbf{E^*} = \begin{bmatrix} e_\alpha^* \\ e_\beta^* \end{bmatrix}$$
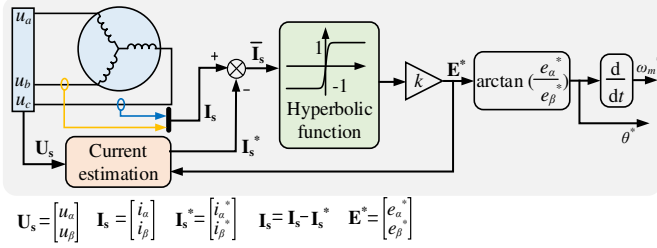
Fig. 4. Structure of the proposed SMO.

$$\frac{dV}{dt} = \underbrace{[-(\frac{R_s}{L_s}\bar{i}_\alpha^2 + \frac{R_s}{L_s}\bar{i}_\beta^2)]}_{\text{term1}} + \tag{13}$$

$$+\underbrace{[\frac{1}{L_s}(e_\alpha - kF(\bar{i}_\alpha))\bar{i}_\alpha + \frac{1}{L_s}(e_\beta - kF(\bar{i}_\beta))\bar{i}_\beta]}_{\text{term2}}$$

Obviously, term1 is less than 0. In order to keep the SMO stable, both term1 and term2 are expected to be less than 0. Therefore, the observer gain can be derived to meet the following criteria:

$$k > \max(|\frac{e_\alpha}{F(\bar{i}_\alpha)}|, |\frac{e_\beta}{F(\bar{i}_\beta)}|) \tag{14}$$

Clearly, the stability condition differs from (5) derived in [29], and it can be noted that k should be much larger because $|F|$ is less than 1 over the BL range. In practice, $\bar{i}_\alpha$ and $\bar{i}_\beta$ are the estimation errors, and referring to the sliding mode theory, they will fluctuate mostly around the sliding surfaces with small variations with the range of tolerance. Define the lower tolerance as ξ, which is:

$$\min(|\bar{i}_\alpha|, |\bar{i}_\beta|) = \xi \tag{15}$$

And the minimum $|F|$ can be rewritten as:

$$\min|F| = \frac{e^{m\xi} - e^{-m\xi}}{e^{m\xi} + e^{-m\xi}} \tag{16}$$

Therefore, the observer gain can be selected as:

$$k = |\frac{3\sqrt{3}C_e'\Psi_f p\omega_{m\_\max}}{2 \cdot \min|F|}| \tag{17}$$

where ω_{m_max} is the maximum speed of the machine and it can be set as the rated value. C_e' is the voltage constant relevant to the motor. The parameter k can guarantee the reachability of the observer, and during the control process, although $\bar{i}_\alpha$ and $\bar{i}_\beta$ might be smaller than ξ when the system gets to the equilibrium state, the proposed SMO can re-converge afterwards.

C. Position and Speed Calculation

An arctangent function is highly suitable for position extraction, and the estimated rotor position θ^* can be calculated by:

$$\theta^* = -\arctan(\frac{e_\alpha^*}{e_\beta^*}) \tag{18}$$

And the estimated angular speed ω_m^* is:

$$\omega_m^* = \frac{d\theta^*}{dt} \tag{19}$$

Overall, the proposed hyperbolic function-based SMO without using LPF and position compensator can be illustrated in Fig.4. In virtue of the new method, the LPF delay issue can be tackled totally.
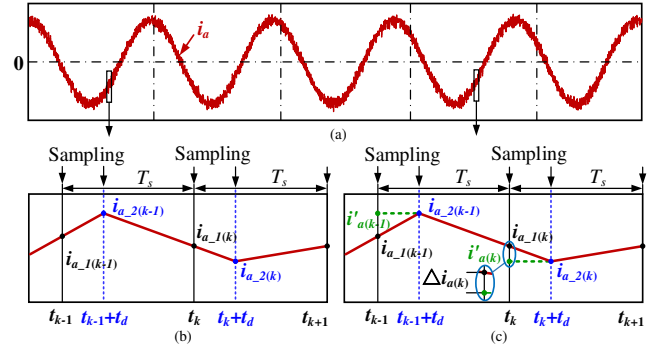

Fig. 5. (a) a-phase current. (b) Delay time calculation. (b) Current compensation.

IV. CALCULATION DELAY PRE-COMPENSATION

Undoubtedly, the calculation delay would lead to lagging control behaviors of VC. To some extent, the root cause of this phenomenon is that the currents sampled at t_k are not equal to the values at $t_k + t_d$. Therefore, an effective way to eliminate the delay effect is to predict the currents at $t_k + t_d$ in advance and use the predicted currents to calculate the rotor position information. This is exactly the so-called pre-compensation method in this paper. For the sake of convenience, this part takes the a-phase current i_a as an example to detail the compensation procedures.

In order to realize the proposed compensation strategy, two assumptions need to be made: 1) the current will shift linearly in each switching period when one voltage vector is selected and applied, and only when another voltage vector is applied will the rate of current change differ in the next period; 2) the computation delay remains constant. Compared to the traditional VC which is characterized by that there is only one sampling point at the beginning of each execution period, the pre-compensation scheme is on the basis of dual sampling. The detailed implementation process consists of the following two phases: delay estimation and compensation.

1) t_d estimation

When estimating t_d, the traditional VC algorithm of which position information is provided by the improved SMO without compensation will be applied. Fig.5 (b) shows the delay computation strategy, and it can be noticed that in each switching period there are two sampling points, one of which is still at the start of a period. The other stands at the actuation moment when the SVPWM algorithm is completed. In Fig.5 (b), the sampling currents over $t_{k-1} \sim t_k$ and $t_k \sim t_{k+1}$ are $i_{a\_1(k-1)}$, $i_{a\_2(k-1)}$ and $i_{a\_1(k)}$, $i_{a\_2(k)}$, respectively. According to the first assumption, the delay can be calculated by:

$$t_d = \frac{|i_{a\_2(k)} - i_{a\_1(k)}|}{|i_{a\_2(k)} - i_{a\_2(k-1)}|} \cdot T_s \tag{20}$$

2) Compensation

Denote the current control period as t_k as well. After obtaining the delay time t_d, the proposed pre-compensation procedures are as follows at t_k:

a) Phase current measurement: use current sensors to detect the real phase currents.

TABLE I
MOTOR AND CONTROL PARAMETERS

Parameter	VALUE	Unit
stator winding resistance R_s	0.6383	Ω
d-axis inductance L_d	2	mH
q-axis inductance L_q	2	mH
the number of pole pairs p	4	-
moment of inertia J	0.013	kg·m^2
viscous coefficient B	0.0035	-
permanent magnet flux linkage Ψ_f	0.085	Wb
DC-link voltage U_{DC}	310	V
switching period T_s	0.0001	s
voltage constant C'_e	1.67	-
rated speed ω_{rated}	314	rad/s
rated torque T_{rated}	5	Nm
rated bus current I_{rated}	6	A
corner speed ω_{cor}	52.3	rad/s

ω_{ref} : reference speed U_{dc}: DC voltage i_{d_ref}, i_{q_ref} : reference currents
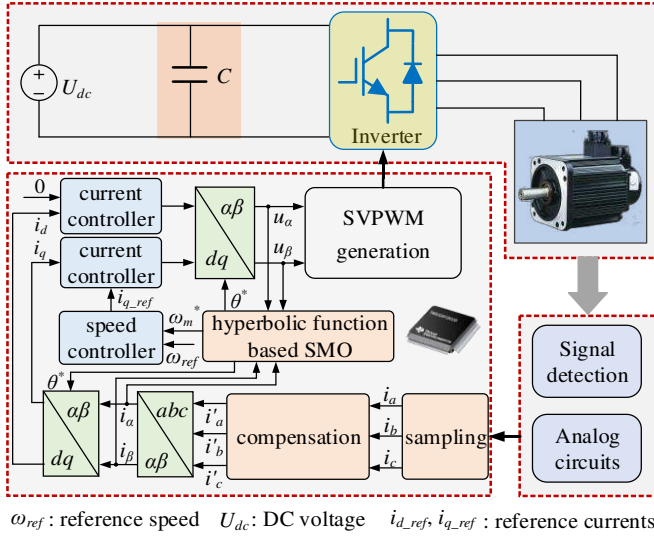
Fig. 6. Block diagram of the delay-suppressed SMO based VC.

b) Compensation: predict the current variation $\triangle i_{a(k)}$ in t_d, as in Fig.5 (c):

$$\Delta i_{a(k)} = \frac{i_{a\_1(k)} - i_{a\_2(k-1)}}{T - t_d} \cdot t_d \qquad (21)$$

$i_{a\_2(k-1)}$ represents the sampling current in the last interval as well, and the a-phase current used for position estimation is:

$$i'_{a(k)} = i_{a\_1(k)} + \Delta i_{a(k)} \qquad (22)$$

Following the above step *b)*, the compensated *b*-phase and *c*-phase current $i'_b(k)$ and $i'_c(k)$ can also be calculated. Then, the compensated phase currents will be used to calculate i_α and i_β by $abc/\alpha\beta$ transformation for obtaining the rotor position information. The block diagram of the delay-suppressed SMO based VC is illustrated in Fig.6.

Interestingly, it can be further noticed that the compensated i_α and i_β are utilized for d, q-axis current computation, which means that the calculation delay effect can also be removed in the current regulation process.

V.   VERIFICATIONS

The performance of the proposed SMO is tested by the means of both simulation and experiments. The motor and control parameters of the PMSM prototype are listed in Table I. Compared to the experimental cases, the simulation is carried out on a personal computer of which processing speed is thousandhold faster than the pratically used digital processors. Therefore, the proposed solution to calculation delay will be only verified by experiments.

A. Simulation Results

a) Analysis on boundary layer

The BL of the hyperbolic function is determined by *m* and it is closely associated with the chattering suppression effect. Theoretically, the narrower the BL is, the larger the total harmonic distortion (THD) caused by chattering will become because the velocity approaching the SS is higher. Fig.7 (a)-(d) illustrate the estimated back EMF under different *m* when the machine operates at the corner speed ω_{cor}, and the THD has a nonlinear relationship versus the BL, which is shown in Fig.7 (e). It can be witnessed that the harmonics takes up 41.5%, 18.6%, 9.5% and 1.7% for *m*=1, 0.25, 0.1 and 0.01, respectively. Although the chattering effect experiences a downward trend as the BL widens, *m* cannot be set to an infinitesimal value because another significant phenomenon is that the amplitude of the estimated back EMF also goes down while the voltage phase remains fixed, which reveals the defect of a switching function with low approaching speed. Unfortunately, this might reduce the robustness and dynamics of the SMO [25]. In practice, we must adjust the parameter *m* to simultaneously guarantee good steady-state and dynamic control performance. What needs to be addressed is that the back EMF of the PMSM will grow as the speed increases while the magnitude of the chattering is nearly invariable, which is conducive to weakening the chattering impact. Thus, the *m* designed at the corner speed can also be suitable over the higher speed range.
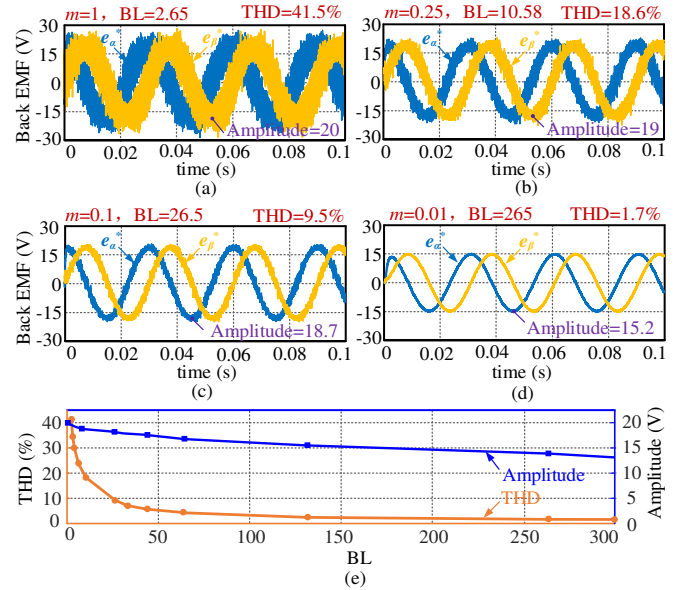

Fig. 7. Chattering effect under different boundary layer or *m*. (a) Back EMF when *m*=1. (b) Back EMF when *m*=0.25. (c) Back EMF when *m*=0.1. (d) Back EMF when *m*=0.01. (e). THD and amplitude of the estimated back EMF.
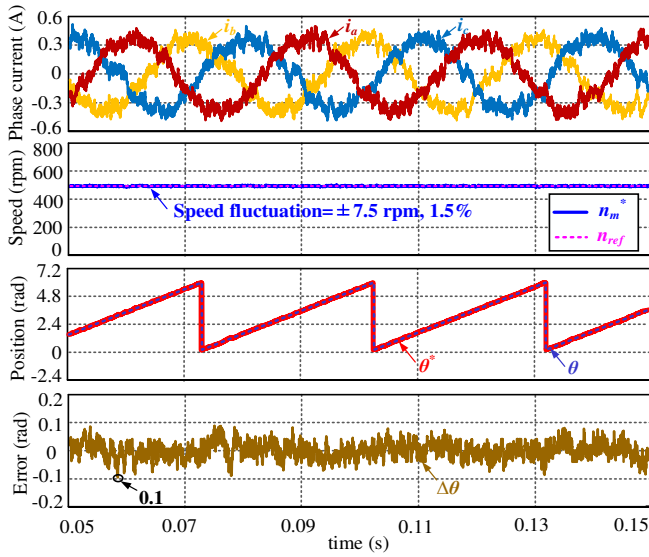
Fig. 8. Steady-state performance at the speed of 500 rpm.

Based on the aforementioned analysis and the test cases, m is set as 0.01 where BL=265 in this paper, and below are the corresponding results.

b) Steady-state performance

Fig.8 illustrates the steady-state performacne characteristics when the motor rotates at the corner speed (reference speed n_{ref}=500 rpm). The amplititude of the symmetrical phase currents is about 0.5 A, representing the no-load current. The rotor speed n_m^* can remain stable at 500 rpm with slight fluctions of ±7.5 rpm (1.5%). Significantly, the proposed SMO shows good position tracking capability according to the third picture in Fig.8, and the position estimation error (PEE) $\Delta\theta$ is within ±0.1 rad. In order to discuss the esitmation and control performance over the high-speed range, a reference speed of
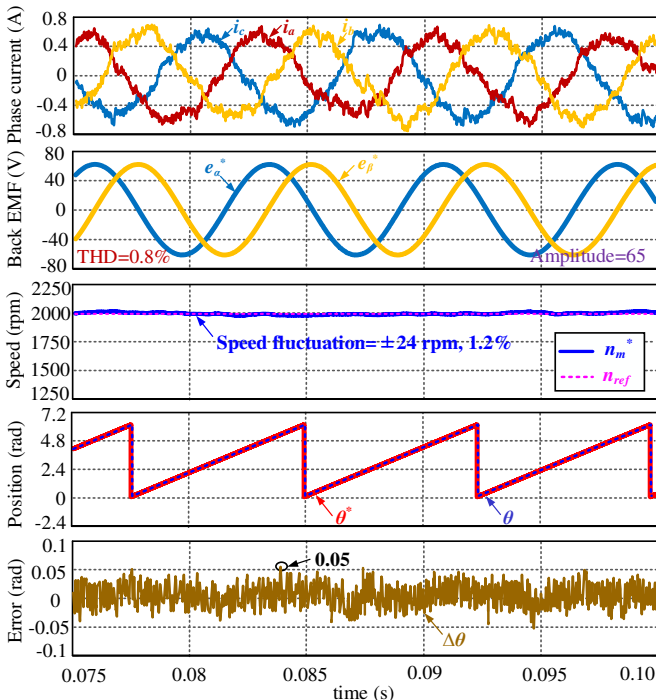

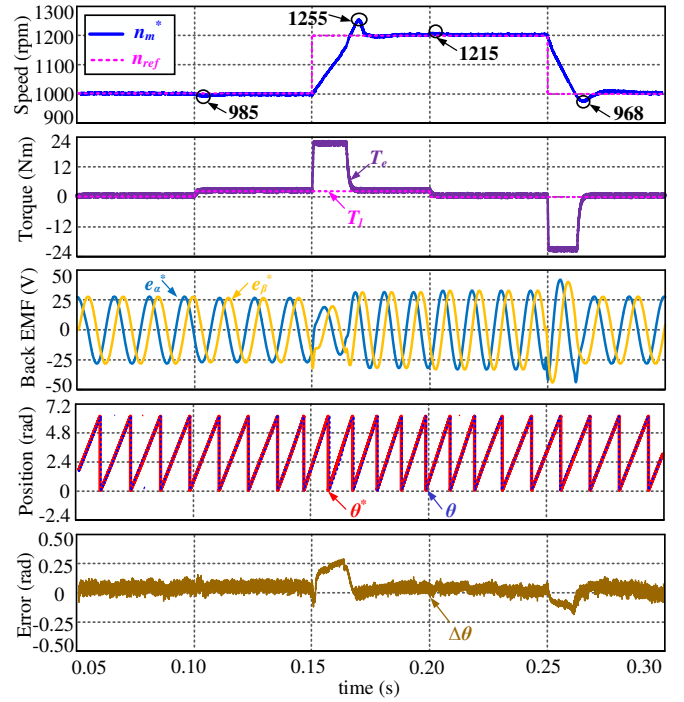Fig. 9. Steady-state performance at the speed of 2000 rpm.

Fig. 10. Dynamic performance.

2000 rpm is set. Fig.9 demonstrates that the no-load current rises by nearly 0.3 A compared to the low-speed case. The back EMF curves verify that the THD caused by chattering decreases as the speed goes up, and it is merely 0.8% when the speed stabilizes at 2000 rpm. Besides, benefitting from the inherent properties of the back EMF based SMO, although the speed fluctuation (SF) becomes ±24 rpm，it just accounts for 1.2% of the reference. As far as the postion is concerned, better estimation accuracy can be witnessed. The estimation error $\Delta\theta$ is approxiamately within ±0.05 rad.

c) Dynamic performance

The dynamic performance tests include speed regulation and sudden load/unload change (as in Fig.10). On the one hand, the reference speed is set to 1000 rpm between 0.05 and 0.15 s initially, and it is 1200 rpm between 0.15 and 0.25 s, after which it is reset as 1000 rpm. On the other hand, a step load torque (T_l) of 2 Nm is applied to the shaft at 0.1 s and it is removed suddenly at 0.2 s.

Firstly, when using the estimated speed and position information to control the system, the machine rotating speed can track the reference well regardless of the acceleration and deceleration process, of which overshoot is 55 rpm (4.6%) and 42 (4.2%) rpm, respectively. Then, when the step load is applied and removed, the speed fluctuates slightly at first, and
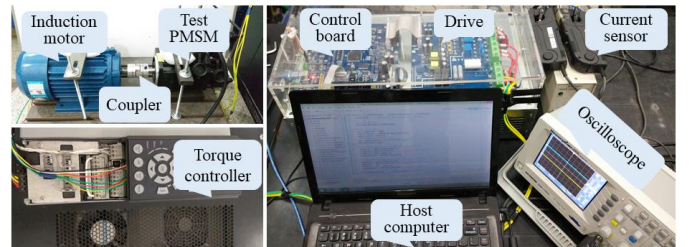

Fig. 11. Experimental setup.

TABLE II
TIME DELAY IN FIFTEEN DIFFERENT PERIODS

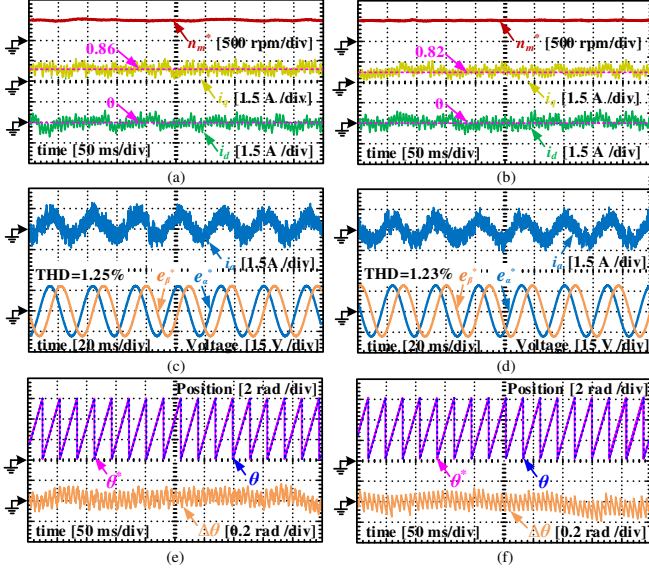| kth period	Delay (ms)	kth period	Delay (ms)	kth period	Delay (ms)
1	0.0334	6	0.0353	11	0.0352
2	0.0332	7	0.0346	12	0.0336
3	0.0343	8	0.0333	13	0.0342
4	0.0343	9	0.0338	14	0.0342
5	0.0340	10	0.0346	15	0.0336

Fig. 12. Experimental steady-state performance at the speed of 500 rpm. (a), (c), (e). SMO without calculation delay compensation. (b), (d), (f). SMO with delay compensation.

then it returns to a stable state quickly. Meanwhile, the machine has a very fast response speed concerning the output electromagnetic torque T_e. This demonstrates that when $m=0.01$, the system still has strong robustness against the external load change. As to the position, the estimation error witnesses an obvious growth up to 0.25 rad when the speed increases, while it is nearly invariable when the load changes.

B. Experimental Results

Experiment is conducted on a three-phase PMSM whose parameters are also consistent with Table I. The experimental equipment is shown in Fig.11. Insulated gate bipolar transistor (IGBT) modules, FP25R12KT3, constitute the voltage inverter with the switching frequency of 10 kHz. The proposed SMO algorithm and the VC control algorithm are implemented on a DSP TMS320F28335 control board. The real rotor position can be detected by a rotary encoder. Hall current sensors, HIOKI 3275 Clamp On Probe, are used to measure the phase currents while the motor d, q-axis currents are calculated by the digital controller. An induction motor driven by an Automation Drive FC 301 with torque control mode, is coupled to the test machine, providing the required load torque.

For the sake of the comparative discussion about the performance before and after delay compensation, the delay time will be tested beforehand according to the proposed pre-compensation approach in this part. Under no load condition, the delay time is measured when the machine is controlled by the VC algorithm. In this process, the improved
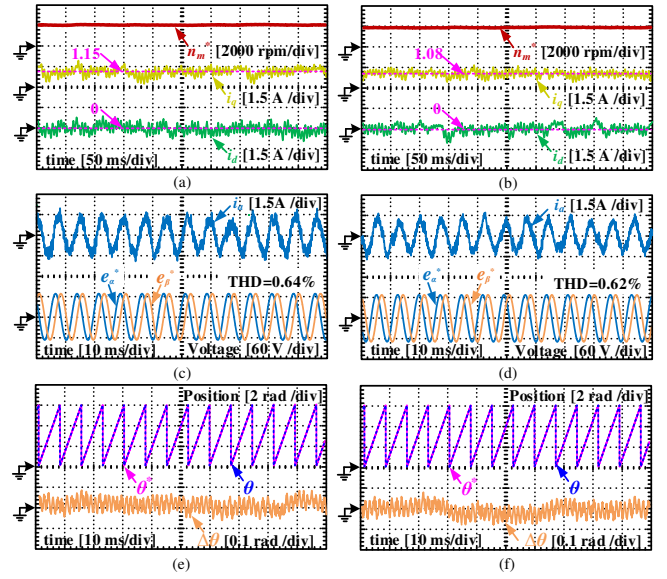

Fig. 13. Experimental steady-state performance at the speed of 2000 rpm. (a), (c), (e). SMO without calculation delay compensation. (b), (d), (f). SMO with delay compensation.

SMO without pre-compensation is employed to detect the rotor position. Table II records the delay value in fifteen different switching periods. It should be noted that the average delay of the test drive system is about 0.0341 ms, accounting for 34.1% of one single cycle. Undoubtedly, this will influence the position estimation accuracy as well as the control performance.

Fig.12 illustrates the steady-state no-load control performance of the improved SMOs with and without calculation delay when the machine rotates at 500 rpm. Firstly, the rotor speed can stabilize at the reference value with pimping fluctuations for both algorithms. Then, because no load is imposed on the machine shaft, the q-axis current is just slightly higher than zero (against viscous resistance) and the d-axis current is about zero. But interestingly, the q-axis current of the
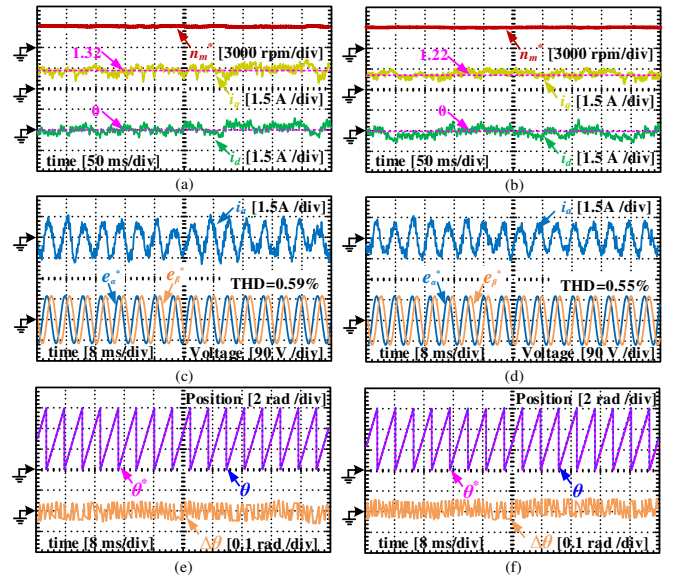

Fig. 14. Experimental steady-state performance at the speed of 3000 rpm. (a), (c), (e). SMO without calculation delay compensation. (b), (d), (f). SMO with delay compensation.
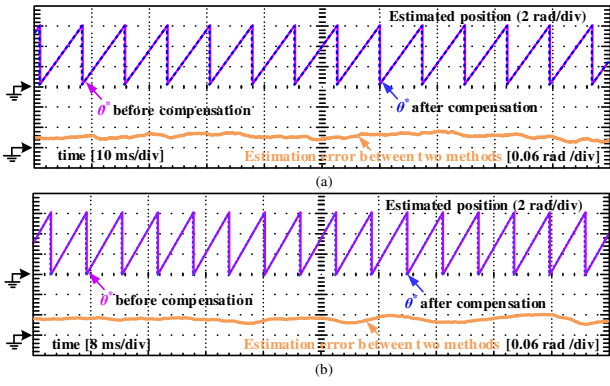
Fig. 15. Difference between the estimated position with and without delay compensation. (a) Speed is 2000 rpm. (b) Speed is 3000 rpm.

SMO with calculation delay pre-compensation reduces by 0.04 A (4.6%) in comparison with the scheme without compensation. Moreover, there are few harmonics in the estimated back EMF, with a THD of 1.25% and 1.23% for the two strategies, respectively. What needs to be observed is that the amplitude of the back EMF is about 18 V, which is closer to the ideal value than the simulation result. Finally, both of the algorithms show marked tracking capability in terms of the position estimation process, as is shown in Fig.12 (e) and (f). The estimation errors are within ±0.2 rad. This is exactly the reason why the machine can be controlled to run well.

To further prove the applicability of the proposed strategies, their steady-state performance characteristics are compared in Fig.13 when the rotor speed is 2000 rpm. In comparison with
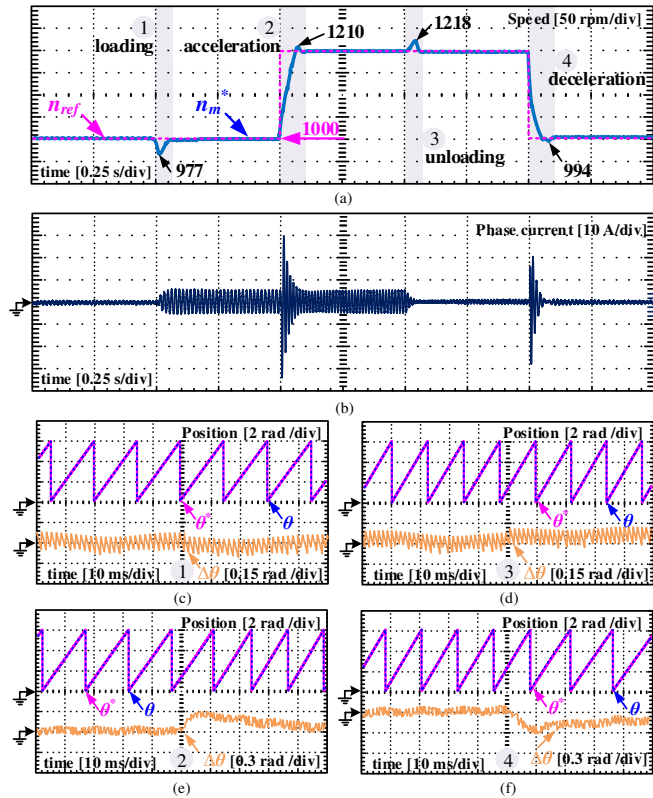

Fig. 16. Experimental dynamic performance. (a) Rotating speed. (b) Phase current. (c) Position under the condition of sudden loading. (d) Position under the condition of sudden unloading. (e) Position under the condition of acceleration. (f) Position under the condition of deceleration.

TABLE III
PRINCIPAL STEADY-STATE PERFORMANCE CHARACTERISTICS

Conditions	Speed (rpm)	SF (rpm)	THD of Back EMF	PEE (rad)
Simulation	500	7.5	1.7%	< 0.1
	2000	24	0.8%	< 0.05
Experiment (non-compensation)	500	35	1.25%	< 0.2
	2000	54	0.64%	< 0.1
Experiment (compensation)	500	33	1.23%	< 0.2
	2000	51	0.62%	< 0.1

Fig.12, at first, the machine has remarkable speed tracking performance as well. Secondly, the viscous force becomes higher as the speed goes up so that the q-axis current rises to over 1 A. But comparatively, the i_q for the compensation algorithm is 1.08 A, 6.1% smaller than that (1.15 A) for the non-compensation method. This means that the effect of calculation delay compensation gets more significant over high speed range. Besides, there are fewer harmonics in the estimated back EMF. The THD is 0.64% and 0.62% for the two strategies, respectively. In this case, the amplitude of the back EMF is about 70 V. As far as the rotor position, the two algorithms show more satisfying performance. The estimation errors are less than ±0.1 rad. When the machine speed rises to 3000 rpm (as in Fig.14), the q-axis current for the compensation algorithm is 7.5% lower than that for the non-compensation method, indicating the impact of calculation delay on the control performance gets more obvious and the compensation effect is better. Much fewer harmonics in the estimated back EMF can be witnessed, with the THDs of 0.59% and 0.55% for the two methods, respectively. Similar to Fig.13, the PEE is less than ±0.1 rad.

In order to intuitively compare the differences between the SMOs with and without compensation means, an extra experiment is designed: use the two algorithms to calculate the rotor position when the motor is controlled by VC strategy, of which the required control information is obtained from the position sensor. In Fig.15, it can be noticed that θ^* before compensation lags those after compensation by about 0.03 and 0.045 rad at the speed of 2000 and 3000 rpm, respectively. In practice, the gap widens over a higher speed range according to the previous analysis, degrading the machine performance.

In accordance with the simulation procedures, the dynamic performance of the improved delay-suppressed SMO is tested (as in Fig.16). When a sudden load of 2 Nm is imposed on the shaft, the machine speed decreases to 977 from 1000 rpm immediately but it recovers to the reference point quickly. By contrast, the machine speed experiences a rise of 18 rpm (1.5%) when the load is removed. When the reference speed changes from 1000 to 1200 rpm, the settling time is about 0.1 s and the overshoot is only 10 rpm (0.8%). In terms of deceleration, an overshoot of 6 rpm can be witnessed. Fig.16 (c) and (d) display the position under the conditions of sudden loading and sudden unloading, respectively. The impact of the load change on the position estimation accuracy can be nearly ignored. Whereas, during acceleration and deceleration, the PEEs will increase. Luckily, after the speed arrives at the setpoint, the estimation

accuracy will resume the normal position (within 0.15 rad).

Finally, Table III summaries the principal steady-state performance characteristics (SF, THD of back EMF and PEE) of the proposed algorithms at the speed of 500 rpm and 2000 rpm to improve the visualization of the novel technique contributions. It can be noted that firstly, the proposed SMO is effective to provide accurate position information for control, and the position estimation results will get slightly better after delay compensation. Secondly, both the experimental and simulation results prove that the chattering effects can be effectively suppressed by using the proposed SMO which does not employ any LPFs.

VI. CONCLUSION

This paper proposes an improved SMO for PMSM sensorless VC method to solve the LPF and calculation delay problems. The main contributions of this paper are as follows:

1) A brand-new hyperbolic function is selected as the switching function following the BL theory. In this case, the LPF can be eliminated because it is found that the chattering phenomenon can be repressed by adjusting the width of BL. Consequently, the proposed SMO succeeds in eliminating the LPF delay.

2) By designing a dual sampling method for the phase current in each switching period, the calculation delay is estimated at first and then, a current-pre-compensation strategy is proposed to compensate the PEE (0.03 and 0.045 rad at the speed of 2000 and 3000 rpm for the test drive, respectively) caused by calculation delay, improving the position estimation accuracy.

The simulation and experimental results prove that the proposed algorithm has good steady-state and dynamic performance. Consequently, it can be concluded that a hyperbolic function is qualified to reduce the chattering of a SMO and simultaneously, the LPF delay can be removed. Further, the proposed calculation pre-compensation approach is able to reject the adverse effects of the delay on the machine performance.

REFERENCES

[1] R. Ni, D. Xu, F. Blaabjerg, K. Lu, G. Wang and G. Zhang, "Square-Wave Voltage Injection Algorithm for PMSM Position Sensorless Control With High Robustness to Voltage Errors," in *IEEE Transactions on Power Electronics*, vol. 32, no. 7, pp. 5425-5437, July 2017.
[2] P. L. Xu and Z. Q. Zhu, "Novel Carrier Signal Injection Method Using Zero-Sequence Voltage for Sensorless Control of PMSM Drives," in *IEEE Transactions on Industrial Electronics*, vol. 63, no. 4, pp. 2053-2061, April 2016.
[3] G. Bisheimer, C. De Angelo, J. Solsona and G. Garcia, "Sensorless PMSM drive with tolerance to current sensor faults," *2008 34th Annual Conference of IEEE Industrial Electronics*, Orlando, FL, 2008, pp. 1379-1384.
[4] C. Gong, Y. Hu, G. Chen, H. Wen, Z. Wang and K. Ni, "A DC-Bus Capacitor Discharge Strategy for PMSM Drive System with Large Inertia and Small System Safe Current in EVs," in *IEEE Transactions on Industrial Informatics*, vol. 15, no. 8, pp. 4709-4718, Aug. 2019
[5] Lu, X. Zhang, Y. Hu, J. Liu, C. Gan and Z. Wang, "Independent Phase Current Reconstruction Strategy for IPMSM Sensorless Control Without Using Null Switching States," in *IEEE Transactions on Industrial Electronics*, vol. 65, no. 6, pp. 4492-4502, June 2018.
[6] J. Liu, C. Gong, Z. Han and H. Yu, "IPMSM Model Predictive Control in Flux-Weakening Operation Using an Improved Algorithm," in *IEEE*

Transactions on Industrial Electronics, vol. 65, no. 12, pp. 9378-9387, Dec. 2018.
[7] Lemmens, P. Vanassche and J. Driesen, "Optimal Control of Traction Motor Drives Under Electrothermal Constraints," in *IEEE Journal of Emerging and Selected Topics in Power Electronics*, vol. 2, no. 2, pp. 249-263, June 2014.
[8] H. Mahmoudi, M. Aleenejad and R. Ahmadi, "Modulated Model Predictive Control for aZ-Source-Based Permanent Magnet Synchronous Motor Drive System," in *IEEE Transactions on Industrial Electronics*, vol. 65, no. 10, pp. 8307-8319, Oct. 2018.
[9] A. H. Abosh, Z. Q. Zhu and Y. Ren, "Reduction of Torque and Flux Ripples in Space Vector Modulation-Based Direct Torque Control of Asymmetric Permanent Magnet Synchronous Machine," in *IEEE Transactions on Power Electronics*, vol. 32, no. 4, pp. 2976-2986, April 2017.
[10] M. Preindl and E. Schaltz, "Sensorless Model Predictive Direct Current Control Using Novel Second-Order PLL Observer for PMSM Drive Systems," in *IEEE Transactions on Industrial Electronics*, vol. 58, no. 9, pp. 4087-4095, Sept. 2011.
[11] G. Wang, L. Yang, G. Zhang, X. Zhang and D. Xu, "Comparative Investigation of Pseudorandom High-Frequency Signal Injection Schemes for Sensorless IPMSM Drives," in *IEEE Transactions on Power Electronics*, vol. 32, no. 3, pp. 2123-2132, March 2017.
[12] G. De Donato, G. Scelba, M. Pulvirenti, G. Scarcella and F. Giulii Capponi, "Low-Cost, High-Resolution, Fault-Robust Position and Speed Estimation for PMSM Drives Operating in Safety-Critical Systems," in *IEEE Transactions on Power Electronics*, vol. 34, no. 1, pp. 550-564, Jan. 2019.
[13] X. Song, J. Fang and B. Han, "High-Precision Rotor Position Detection for High-Speed Surface PMSM Drive Based on Linear Hall-Effect Sensors," in *IEEE Transactions on Power Electronics*, vol. 31, no. 7, pp. 4720-4731, July 2016.
[14] X. Liu, C. Liu and P. W. T. Pong, "Velocity Measurement Technique for Permanent Magnet Synchronous Motors Through External Stray Magnetic Field Sensing," in *IEEE Sensors Journal*, vol. 18, no. 10, pp. 4013-4021, 15 May15, 2018.
[15] S. Chen, G. Liu and L. Zhu, "Sensorless Control Strategy of a 315 kW High-Speed BLDC Motor Based on a Speed-Independent Flux Linkage Function," in *IEEE Transactions on Industrial Electronics*, vol. 64, no. 11, pp. 8607-8617, Nov. 2017.
[16] D. Nguyen, R. Dutta, M. F. Rahman and J. E. Fletcher, "Performance of a Sensorless Controlled Concentrated-Wound Interior Permanent-Magnet Synchronous Machine at Low and Zero Speed," in *IEEE Transactions on Industrial Electronics*, vol. 63, no. 4, pp. 2016-2026, April 2016.
[17] W. Li, J. Fang, H. Li and J. Tang, "Position Sensorless Control Without Phase Shifter for High-Speed BLDC Motors With Low Inductance and Nonideal Back EMF," in *IEEE Transactions on Power Electronics*, vol. 31, no. 2, pp. 1354-1366, Feb. 2016.
[18] M. Seilmeier and B. Piepenbreier, "Sensorless Control of PMSM for the Whole Speed Range Using Two-Degree-of-Freedom Current Control and HF Test Current Injection for Low-Speed Range," in *IEEE Transactions on Power Electronics*, vol. 30, no. 8, pp. 4394-4403, Aug. 2015.
[19] E. Al-nabi, B. Wu, N. R. Zargari and V. Sood, "Sensorless Control of CSC-Fed IPM Machine for Zero- and Low-Speed Operations Using Pulsating HFI Method," in *IEEE Transactions on Industrial Electronics*, vol. 60, no. 5, pp. 1711-1723, May 2013.
[20] S. K. Kommuri, S. B. Lee and K. C. Veluvolu, "Robust Sensors-Fault-Tolerance With Sliding Mode Estimation and Control for PMSM Drives," in *IEEE/ASME Transactions on Mechatronics*, vol. 23, no. 1, pp. 17-28, Feb. 2018.
[21] T. Bernardes, V. F. Montagner, H. A. Gründling and H. Pinheiro, "Discrete-Time Sliding Mode Observer for Sensorless Vector Control of Permanent Magnet Synchronous Machine," *in IEEE Transactions on Industrial Electronics*, vol. 61, no. 4, pp. 1679-1691, April 2014.
[22] Y. Fan, L. Zhang, M. Cheng and K. T. Chau, "Sensorless SVPWM-FADTC of a New Flux-Modulated Permanent-Magnet Wheel Motor Based on a Wide-Speed Sliding Mode Observer," in *IEEE Transactions on Industrial Electronics*, vol. 62, no. 5, pp. 3143-3151, May 2015.
[23] Q. Lu, X. Zhu, L. Quan, Y. Zuo and S. Du, "Rotor position estimation scheme with harmonic ripple attenuation for sensorless controlled permanent magnet synchronous motors," in *IET Electric Power Applications*, vol. 12, no. 8, pp. 1200-1206, 9 2018.

[24] Jingbo Liu, Jiangang Hu and Longya Xu, "Sliding Mode Observer for Wide Speed Range Sensorless Induction Machine Drives: Considerations for Digital Implementation," I*EEE International Conference on Electric Machines and Drives*, 2005., San Antonio, TX, 2005, pp. 300-307.

[25] Y. Feng, J. Zheng, X. Yu and N. V. Truong, "Hybrid Terminal Sliding-Mode Observer Design Method for a Permanent-Magnet Synchronous Motor Control System," in *IEEE Transactions on Industrial Electronics*, vol. 56, no. 9, pp. 3424-3431, Sept. 2009.

[26] D. Liang, J. Li, R. Qu and W. Kong, "Adaptive Second-Order Sliding-Mode Observer for PMSM Sensorless Control Considering VSI Nonlinearity," in *IEEE Transactions on Power Electronics*, vol. 33, no. 10, pp. 8994-9004, Oct. 2018.

[27] F. Dinuzzo and A. Ferrara, "Higher Order Sliding Mode Controllers With Optimal Reaching," in *IEEE Transactions on Automatic Control*, vol. 54, no. 9, pp. 2126-2136, Sept. 2009.

[28] X. Zhang, "Sensorless Induction Motor Drive Using Indirect Vector Controller and Sliding-Mode Observer for Electric Vehicles," in *IEEE Transactions on Vehicular Technology*, vol. 62, no. 7, pp. 3010-3018, Sept. 2013.

[29] H. Kim, J. Son and J. Lee, "A High-Speed Sliding-Mode Observer for the Sensorless Speed Control of a PMSM," in *IEEE Transactions on Industrial Electronics*, vol. 58, no. 9, pp. 4069-4077, Sept. 2011.

[30] A. Saghafinia, H. W. Ping, M. N. Uddin and K. S. Gaeid, "Adaptive Fuzzy Sliding-Mode Control Into Chattering-Free IM Drive," in *IEEE Transactions on Industry Applications*, vol. 51, no. 1, pp. 692-701, Jan.-Feb. 2015.

[31] J. R. Fischer, S. A. González, M. A. Herrán, M. G. Judewicz and D. O. Carrica, "Calculation-Delay Tolerant Predictive Current Controller for Three-Phase Inverters," in *IEEE Transactions on Industrial Informatics*, vol. 10, no. 1, pp. 233-242, Feb. 2014.

[32] T. Jin, X. Shen, T. Su and R. C. C. Flesch, "Model Predictive Voltage Control Based on Finite Control Set With Computation Time Delay Compensation for PV Systems," in *IEEE Transactions on Energy Conversion*, vol. 34, no. 1, pp. 330-338, March 2019.

[33] L. Sepulchre, M. Fadel and M. Pietrzak-David, "Improvement of the digital control of a high speed PMSM for vehicle application," *2016 Eleventh International Conference on Ecological Vehicles and Renewable Energies (EVER)*, Monte Carlo, 2016, pp. 1-9.

[34] P. Cortes, J. Rodriguez, C. Silva and A. Flores, "Delay Compensation in Model Predictive Current Control of a Three-Phase Inverter," in *IEEE Transactions on Industrial Electronics*, vol. 59, no. 2, pp. 1323-1325, Feb. 2012.
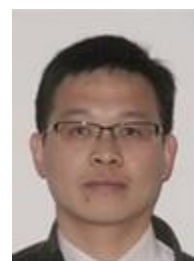
Jinqiu Gao was born in Shannxi province in P.R. China, on January 07, 1996. She received the B.Eng. degree in electrical engineering from Northwestern Polytechnical University, Xi'an, China, in 2017. Currently, she is a Master student with the major of Electrical Engineering in the School of Automation, Northwestern Polytechnical University, Xi'an, China. Her research interests include electrical machines design and drives, power electronics and motion control.

Yangang Wang (M'14-SM'16) received PhD degree in Microelectronics and Solid-State Electronics from Peking University in 2007. He joined the R&D Centre of CRRC Dynex Semiconductor Ltd in the UK as a Principal Engineer in 2012, and is currently in the leading role of the department responsible for development of advanced Si and WBG power semiconductor products. Dr. Wang is a senior member of IEEE, member of IET and a Chartered Engineer of the UK. He has more than 20-year research and development work experience on Microelectronics and Power Electronics. His current research and development activities include design/simulation, packaging, test/characterization, failure analysis, reliability and lifetime prediction etc for power Si and WBG semiconductor devices.

Chao Gong (S'19) was born in Shandong province in P.R. China, on February 22, 1991. He received the B.Eng. and the M.Eng degree in electrical engineering from Northwestern Polytechnical University, Xi'an, China, in 2014 and 2016, respectively. Currently, he is a PHD student with the major of Electrical Engineering in the Department of Electrical Engineering and Electronics of University of Liverpool, Liverpool, the UK. His research interests include electrical machines design and drives, power electronics and motion control.

Liming Yan (S'18) was born in Shaanxi, China, in 1988. He received the B.S. degree in software engineering at Chang'an university, China, in 2011, and the M.S. degree in electric machine and electric apparatus at Shenyang University of Technology, China, in 2014, and the Ph.D. degree in electrical engineering at Northwestern Polytechnical University, China, in 2019. Currently he is working at Chang'an university, China. His research interests include model predictive control of power electronics and electrical drives.

Yihua Hu (M'13-SM'15) received the B.S. degree in electrical motor drives in 2003, and the Ph.D. degree in power electronics and drives in 2011. Between 2011 and 2013, he was with the College of Electrical Engineering, Zhejiang University as a Postdoctoral Fellow. Between 2013 and 2015, he worked as a Research Associate at the power electronics and motor drive group, the University of Strathclyde. Currently, he is a Lecturer at the Department of Electrical Engineering and Electronics, University of Liverpool (UoL). He has published 65 papers in IEEE Transactions journals. His research interests include renewable generation, power electronics converters & control, electric vehicle, more electric ship/aircraft, smart energy system and non-destructive test technology. He is the associate editor of IET Renewable Power Generation, IET Intelligent Transport Systems and Power Electronics and Drives.